Journal of Nanophotonics

SPIEDigitalLibrary.org/jnp

Plasmon polariton deceleration in graphene structures

Konstantin G. Batrakov
Vasily A. Saroka
Sergey A. Maksimenko
Christian Thomsen

SPIE

Plasmon polariton deceleration in graphene structures

Konstantin G. Batrakov,[a] Vasily A. Saroka,[a] Sergey A. Maksimenko,[a] and Christian Thomsen[b]

[a]Belarusian State University, Institute for Nuclear Problems, Bobruiskaya 11, 220030 Minsk, Belarus
kgbatrakov@gmail.com

[b]Technische Universität Berlin, Institut für Festkörperphysik, Hardenbergstr. 36, D-10623 Berlin, Germany

Abstract. Surface plasmon-polariton waves with low-phase speed in carbon nanostructures can be utilized for the generation of coherent terahertz radiation through the Čerenkov mechanism, the effect being especially pronounced in bilayer and multilayer graphene. Using the many-body formalism and the tight-binding approach, we derived the dispersion equations of the surface plasmon-polariton waves in graphene. In single-layer graphene, the phase speed is about three to five times smaller than the speed of light in a vacuum. In bilayer graphene, inter-layer electron tunneling suppresses the reduction of the phase speed. Reduction of the phase speed by as much as 300 times is possible in a graphene structure with two spatially expanded monolayers, because inter-layer tunneling is suppressed, and the interlayer distance can be used to tune the plasmon frequency and the phase speed.
[DOI: 10.1117/1.JNP.6.061719]

Keywords: graphene; graphene bilayer; surface plasmon-polariton wave; slowing down.

Paper 12115SS received Aug. 16, 2012; revised manuscript received Oct. 23, 2012; accepted for publication Oct. 23, 2012; published online Dec. 5, 2012.

1 Introduction

Graphene, graphene bilayer, and other graphene structures are very interesting objects with many applications in different science and practical areas. The plasmon-polariton waves in graphene are generating significant interest. As graphene is a two-dimensional (2-D) structure, the plasmon-polariton waves essentially have surface character. Surface plasmon-polariton (SPP) waves can give rise to the field of nanophotonics and subwavelength wave localization. A very important and interesting application is the generation in graphene of terahertz (THz) radiation. This can be utilized for the design of compact sources of THz radiation, a problem of great scientific and practical interest. There are very few commercially available instruments for the THz frequency region and very often they lack the precision required for performing accurate measurements. One of the latest trends is the use of single-wall carbon nanotubes (SWNTs), cylindrical molecules with nanometer diameter and micrometer length,[1–3] as building blocks of novel THz devices.[4–9] Proposals to realize a THz plasmon oscillator on the basis of graphene were also recently made in Ref. 10. The Čerenkov and channeling radiation mechanisms in nanotubes were proposed in Refs. 11–15 for the electromagnetic wave generation. The idea has been extended to multiwall nanotubes and multilayer graphene in Ref. 16 without accounting for the inter-layer tunneling. Here we show the important role of the latter mechanism.

The slowing of the electromagnetic wave is required for the realization of Čerenkov-type synchronism. As was shown earlier,[17] the single-wall nanotube can slow the surface electromagnetic wave up to 100 times. Nevertheless, to provide the effective synchronization between electromagnetic wave and electron current in nanotubes or graphene structures, a stronger slowing is required. The use of two-wall nanotubes has been proposed as a way to overcome the problem. [16] However, the difference of the radii in a two-wall nanotube prevent significant deceleration. This paper discusses plane graphene structures. It is shown that the ability to slow the wave in such

0091-3286/2012/$25.00 © 2012 SPIE

structures can essentially exceed the slowing in nanotubes. The dielectric function and plasmon modes in graphene and graphene bilayer were considered in Refs. 18–20. However, in these works the graphene bilayer was considered as an infinitely thin sheet of material with the conductivity $\sigma(\mathbf{q}, \omega)$. As different from that, we use a three-dimensional (3-D) approach for SPP wave calculations.

The paper is organized in the following way. After a brief introduction in Sec. 1, the basic equations describing SPP wave dynamics based on Maxwell equations for fields and operator Heisenberg equations for many-body electron system are derived in Sec. 2 in the tight binding approach for wave functions in multilayer graphene. Resulting calculations and discussions for the slowing in single, bilayer, and spatially separated double-layer graphene are presented in Secs. 3 and 4, followed by the concluding Sec. 5.

2 Basic Equations

In this paper, we consider the interaction between electromagnetic field and electron system in graphene structure (single, bilayer, multilayer graphene). A self-consistent system describing this system includes the electromagnetic field equations with charge and charge current densities in the right-hand parts as a source, and the electron motion equation with electromagnetic field in the right-hand part of equation as a force. The equations for scalar and vector potentials have the form:

$$\nabla^2\mathbf{A} - \frac{1}{c^2}\frac{\partial^2\mathbf{A}}{\partial t^2} = -\frac{4\pi}{c}\mathbf{j}(\mathbf{r}, t), \qquad \nabla^2\Phi - \frac{1}{c^2}\frac{\partial^2\Phi}{\partial t^2} = -4\pi\rho(\mathbf{r}, t). \tag{1}$$

The Lorentz gauge is used when Eq. (1) is written:

$$\frac{1}{c}\frac{\partial\Phi}{\partial t} + \nabla\mathbf{A} = 0. \tag{2}$$

In this paper, we consider the situation when the electromagnetic field is rather large, i.e., the condition:

$$E \gg \sqrt{\hbar c}\left(\frac{\omega}{c}\right)^2 \tag{3}$$

is fulfilled,[21] where E is the electromagnetic field strength, ω is its angular frequency, and c is the speed of light in vacuum. In this case, the electromagnetic wave has a classical character and is described by the classical wave equations [Eq. (1)]. The electron motion is governed by the Schrödinger equation, therefore the quantities $\mathbf{j}(\mathbf{r}, t)$ $\rho(\mathbf{r}, t)$ in the right-hand part of the field [Eq. (1)] are the operators of the current density and the charge density averaged over the quantum states of the electron system. Dynamics of the electron system in the electromagnetic field are described by the Hamiltonian:

$$\hat{H} = \sum E_{\mathbf{k}s}\hat{b}^{\dagger}_{\mathbf{k}s}\hat{b}_{\mathbf{k}s} + e\int \Phi(\mathbf{r}, t)\hat{\psi}^{\dagger}(\mathbf{r}, t)\hat{\psi}(\mathbf{r}, t)\mathrm{d}\mathbf{r}$$
$$-\frac{e}{2mc}\int \hat{\psi}^{\dagger}(\mathbf{r}, t)[\mathbf{A}(\mathbf{r}, t)\hat{\mathbf{p}} + \hat{\mathbf{p}}\mathbf{A}(\mathbf{r}, t)]\hat{\psi}(\mathbf{r}, t)\mathrm{d}\mathbf{r}. \tag{4}$$

The term proportional to the vector-potential squared has been neglected in Eq. (4). Here, $E_{\mathbf{k}s}$ is the electron energy characterized by the the quasi-momentum $\mathbf{k}$ and the electron subsystem band number s. The electron quantum field operator is given by:

$$\hat{\psi}(\mathbf{r}, t) = \sum \psi_{\mathbf{k}s}(\mathbf{r})\hat{b}_{\mathbf{k}s}(t), \tag{5}$$

where $\psi_{\mathbf{k}s}$ is the electron Bloch wave function in the multilayer graphene structure, $\hat{b}_{\mathbf{k}s}$, $\hat{b}^{\dagger}_{\mathbf{k}s}$ are the annihilation and creation operators for the electron with the quasi-momentum $\mathbf{k}$ in the s band,

$\hat{\mathbf{p}}$ is the quantum momentum operator. The Heisenberg equations for the annihilation/creation operators corresponding to the Hamiltonian [Eq. (4)] have the form as follows:

$$\dot{\hat{b}}_{\mathbf{k}s}(t) = -\frac{i}{\hbar}E_{\mathbf{k}s}\hat{b}_{\mathbf{k}s}(t) - \frac{i}{\hbar}e\sum_{1}\left\langle \mathbf{k}s\left|\Phi(\mathbf{r},\omega) - \frac{1}{2mc}[\mathbf{A}(\mathbf{r},\omega)\hat{\mathbf{p}} + \hat{\mathbf{p}}\mathbf{A}(\mathbf{r},\omega)]\right|\mathbf{k}_1 s_1\right\rangle \hat{b}_{\mathbf{k}_1 s_1}(t), \tag{6}$$

$$\dot{\hat{b}}^{\dagger}_{\mathbf{k}s}(t) = \frac{i}{\hbar}E_{\mathbf{k}s}\hat{b}^{\dagger}_{\mathbf{k}s}(t) + \frac{i}{\hbar}e\sum_{1}\left\langle \mathbf{k}_1 s_1\left|\Phi(\mathbf{r},\omega) - \frac{1}{2mc}[\mathbf{A}(\mathbf{r},\omega)\hat{\mathbf{p}} + \hat{\mathbf{p}}\mathbf{A}(\mathbf{r},\omega)]\right|\mathbf{k}s\right\rangle \hat{b}^{\dagger}_{\mathbf{k}_1 s_1}(t). \tag{7}$$

Hereafter, symbols 1 and 2 in summation denote summation over the sets $\mathbf{k}_1 s_1$ and $\mathbf{k}_2 s_2$, respectively. Considering electromagnetic field in Eqs. (6) and (7) as a perturbation, in the linear approximation we come to the following self-consistent equations for the electromagnetic potentials:

$$\begin{aligned}\left(\frac{\mathrm{d}^2}{\mathrm{d}z^2} - \mathbf{q}^2 + \frac{\omega^2}{c^2}\right)\mathbf{A} = &-\frac{2\pi e^2}{mc}\sum_{1,2}\int \mathrm{d}\mathbf{r}_\perp e^{-i\mathbf{q}\mathbf{r}_\perp}(\psi^*_{\mathbf{k}_2 s_2}\hat{\mathbf{p}}\psi_{\mathbf{k}_1 s_1} - \hat{\mathbf{p}}\psi^*_{\mathbf{k}_2 s_2}\psi_{\mathbf{k}_1 s_1}) \\ &\times\frac{\left\langle \mathbf{k}_1 s_1\left|\Phi(\mathbf{r},\omega) - \frac{1}{2mc}[\mathbf{A}(\mathbf{r},\omega)\hat{\mathbf{p}} + \hat{\mathbf{p}}\mathbf{A}(\mathbf{r},\omega)]\right|\mathbf{k}_2 s_2\right\rangle}{\omega + E_{\mathbf{k}_2 s_2} - E_{\mathbf{k}_1 s_1}}(n_{\mathbf{k}_2 s_2} - n_{\mathbf{k}_1 s_1}) \\ &+\frac{4\pi e^2}{mc^2}\sum_{1}\int \mathrm{d}\mathbf{r}_\perp e^{-i\mathbf{q}\mathbf{r}_\perp}\psi^*_{\mathbf{k}_1 s_1}\psi_{\mathbf{k}_1 s_1}\mathbf{A}(\mathbf{r},\omega)\langle 0|\hat{b}^{(0)\dagger}_{\mathbf{k}_1 s_1}\hat{b}^{(0)}_{\mathbf{k}_1 s_1}|0\rangle,\end{aligned} \tag{8}$$

$$\begin{aligned}\left(\frac{\mathrm{d}^2}{\mathrm{d}z^2} - \mathbf{q}^2 + \frac{\omega^2}{c^2}\right)\Phi = &-4\pi e^2\sum_{1,2}\int \mathrm{d}\mathbf{r}_\perp e^{-i\mathbf{q}\mathbf{r}_\perp}\psi^*_{\mathbf{k}_2 s_2}\psi_{\mathbf{k}_1 s_1} \\ &\times\frac{\left\langle \mathbf{k}_1 s_1\left|\Phi(\mathbf{r},\omega) - \frac{1}{2mc}[\mathbf{A}(\mathbf{r},\omega)\hat{\mathbf{p}} + \hat{\mathbf{p}}\mathbf{A}(\mathbf{r},\omega)]\right|\mathbf{k}_2 s_2\right\rangle}{\omega + E_{\mathbf{k}_2 s_2} - E_{\mathbf{k}_1 s_1}}(n_{\mathbf{k}_2 s_2} - n_{\mathbf{k}_1 s_1}).\end{aligned} \tag{9}$$

Here $n_{\mathbf{k}_2 s_2} - n_{\mathbf{k}_1 s_1} = \langle 0|\hat{b}^{(0)\dagger}_{\mathbf{k}_2 s_2}\hat{b}^{(0)}_{\mathbf{k}_2 s_2} - \hat{b}^{(0)\dagger}_{\mathbf{k}_1 s_1}\hat{b}^{(0)}_{\mathbf{k}_1 s_1}|0\rangle$, $\hat{b}^{(0)}_{\mathbf{k}s}$, $\hat{b}^{(0)\dagger}_{\mathbf{k}s}$ are unperturbed operators, $|0\rangle$ is the many-body state of the electron subsystem, and $n_{\mathbf{k}_i s_i}$ are quantum occupation numbers. When deriving Eqs. (8) and (9), the Fourier transforms of the potentials over two space coordinates parallel to the graphene layers and over time have been performed. The axis z is normal to the graphene surface. In the left-hand parts of the above equations, the potentials $\mathbf{A}$ and Φ denote the Fourier-transformed potentials: $\mathbf{A} \equiv \mathbf{A}(z,\mathbf{q},\omega)$ and $\Phi \equiv \Phi(z,\mathbf{q},\omega)$.

Equations (8) and (9) with Eqs. (6) and (7) describe a graphene structure with an arbitrary number of layers. For deriving of graphene dispersion properties, a ground quantum state $|0\rangle$ that is described by Fermi distribution function is usually used. However, the same equations can be applied in the case of an excited electron system, for example in the case when the electron current moves over the ground state. Then the state $|0,n_b\rangle$ can be used in the matrix elements of Eqs. (8) and (9) right hand parts instead of $|0\rangle$. The numbers n_b denote the electron excited part of the electron system, directed electron flow for example. The right side of Eqs. (8) and (9) contains expressions of wave functions $|\mathbf{k}s\rangle = \psi_{\mathbf{k}s}$, which should be defined. In the tight-binding approximation, the electron wave-function in a multilayer graphene is given by Ref. 22:

$$\psi_{\mathbf{k}s} = \sum_i [c^{A_i}_{\mathbf{k}s}\psi^{A_i}_{\mathbf{k}}(\mathbf{r}) + c^{B_i}_{\mathbf{k}s}\psi^{B_i}_{\mathbf{k}}(\mathbf{r})], \tag{10}$$

where $\psi^{A_i}_{\mathbf{k}}(\mathbf{r})$ and $\psi^{B_i}_{\mathbf{k}}(\mathbf{r})$ are the tight-binding Bloch functions of i'th layer corresponding to carbon atoms in two graphene sublattices denoted by indexes A and B. These functions are represented as:

$$\psi_{\mathbf{k}}^{A_i}(\mathbf{r}) = \frac{1}{\sqrt{N}} \sum_{A_i} \phi_A(\mathbf{r} - \mathbf{r}_{A_i}) \exp(i\mathbf{k}\mathbf{r}_{A_i})$$
$$\psi_{\mathbf{k}}^{B_i}(\mathbf{r}) = \frac{1}{\sqrt{N}} \sum_{B_i} \phi_B(\mathbf{r} - \mathbf{r}_{B_i}) \exp(i\mathbf{k}\mathbf{r}_{B_i}). \tag{11}$$

Here, ϕ_A and ϕ_B are the atomic wave functions of carbon atoms in sublattices A and B, respectively, and $\mathbf{r}_{A_i}$ and $\mathbf{r}_{B_i}$ are the positions of atoms in i'th layer; and N is the number of unit cells. Coefficients $c_{\mathbf{k}s}^{A_i}$ and $c_{\mathbf{k}s}^{B_i}$ in Eq. (11) are derived by the tight-binding method.[22] The method is fully applied to graphene with any layer quantity ($i = 1, \ldots, n$). For the graphene bilayer ($i = 1$, 2) shown schematically in Fig. 1, the tight-binding method leads to four solutions derived from the Schrödinger equation using Eq. (11). In that case we arrive at a four-dimensional matrix equation:

$$\mathcal{A}\mathbf{c} = 0, \tag{12}$$

where

$$\mathcal{A} = \begin{pmatrix} E_0 + \Delta - E & (\gamma_0' - s_{12}E)f & \gamma_1' - s_{13}E & (\gamma_4' - s_{14}E)f^* \\ (\gamma_0' - s_{12}E)f^* & E_0 - E & (\gamma_4' - s_{23}E)f^* & (\gamma_3' - s_{24}E)f \\ \gamma_1' - s_{13}E & (\gamma_4' - s_{23}E)f & E_0 + \Delta - E & (\gamma_0' - s_{34}E)f^* \\ (\gamma_4' - s_{14}E)f & (\gamma_3' - s_{24}E)f^* & (\gamma_0' - s_{34}E)f & E_0 - E \end{pmatrix}, \tag{13}$$

and $\mathbf{c}$ is the column vector given as the transposition of the row vector

$$(\, c_{\mathbf{k}s}^{A_1} \quad c_{\mathbf{k}s}^{B_1} \quad c_{\mathbf{k}s}^{A_2} \quad c_{\mathbf{k}s}^{B_2} \,). \tag{14}$$

The overlap integrals s_{ij} are usually neglected in this system.[2,22] The values of parameters γ_i, E_0 are given in article devoted to analysis of graphene electron eigenstates and eigenvalues[22] (for graphene bilayer $E_0 = -0.0206$ eV, $\gamma_0' = 3.12$ eV, $\gamma_1' = 0.377$ eV, $\gamma_3' = 0.29.12$ eV, $\gamma_4' = -0.120$ eV), and function $f \equiv f(k_x, k_y) = \exp(ik_x a/\sqrt{3}) + 2\exp(-ik_x a/2\sqrt{3})\cos(k_y a/2)$ (a is the in-plane lattice parameter). Following Ref. 22, further we neglect overlap integrals s_{ij}. The functions ϕ_A and ϕ_B were chosen as

$$\phi_A = \phi_B = \frac{1}{4\sqrt{2\pi}} (Z/a_B)^2 (Zr/a_B) \exp(-Zr/a_B) \cos\theta. \tag{15}$$

Here Z is atom charge ($Z = 6$ for carbon), and a_B is Bohr radius. Equation (12) for graphene bilayer gives four different solutions and four eigenstates. The substitution of the tight-binding form of the electron wave functions for multilayer graphene into Eqs. (8) and (9) gives:

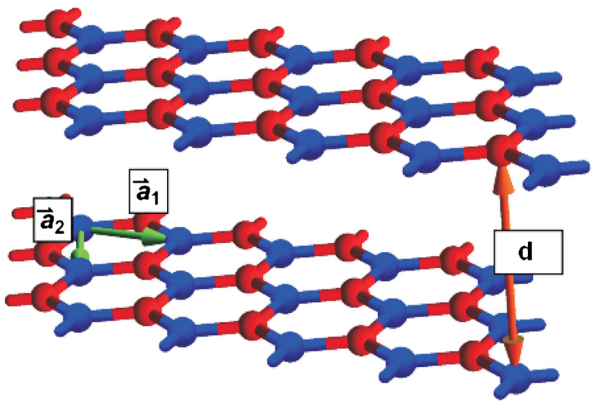

Fig. 1 The crystal structure of graphene bilayer. $\vec{a}_1$, $\vec{a}_2$ are the translational vectors, and d is the distance between graphene layers.

$$\left(\frac{\mathrm{d}^2}{\mathrm{d}z^2}-\mathbf{q}^2+\frac{\omega^2}{c^2}\right)\mathbf{A}(z,\mathbf{q},\omega)=\frac{2\pi e^2}{mcS}\sum_{1,2,i}\delta_{\mathbf{k}_2+\mathbf{q},\mathbf{k}_1}(n_{\mathbf{k}_2 s_2}-n_{\mathbf{k}_1 s_1}) \times\sum_{\alpha}(c^{B_i*}_{\mathbf{k}_2 s_2}c^{A_i}_{\mathbf{k}_1 s_1}e^{-i\mathbf{k}_2\delta_\alpha}-c^{A_i*}_{\mathbf{k}_2 s_2}c^{B_i}_{\mathbf{k}_1 s_1}e^{i\mathbf{k}_1\delta_\alpha})\mathbf{j}^{A_iB_i}_{\alpha}(z,\mathbf{q})B^{s_1 s_2}_{\mathbf{k}_1\mathbf{k}_2}(\mathbf{q},\omega), \quad (16)$$

$$\left(\frac{\mathrm{d}^2}{\mathrm{d}z^2}-\mathbf{q}^2+\frac{\omega^2}{c^2}\right)\Phi(z,\mathbf{q},\omega)=-\frac{4\pi e^2}{S}\sum_{1,2,i}\delta_{\mathbf{k}_2+\mathbf{q},\mathbf{k}_1}(n_{\mathbf{k}_2 s_2}-n_{\mathbf{k}_1 s_1}) \times[c^{A_i*}_{\mathbf{k}_2 s_2}c^{A_i}_{\mathbf{k}_1 s_1}F_{A_i}(z,-\mathbf{q})+c^{B_i*}_{\mathbf{k}_2 s_2}c^{B_i}_{\mathbf{k}_1 s_1}F_{B_i}(z,-\mathbf{q})]B^{s_1 s_2}_{\mathbf{k}_1\mathbf{k}_2}(\mathbf{q},\omega), \quad (17)$$

$$\frac{-i\omega}{c}\Phi(z,\mathbf{q},\omega)+i\mathbf{q}\mathbf{A}(z,\mathbf{q},\omega)+\frac{\mathrm{d}A_z(z,\mathbf{q},\omega)}{\mathrm{d}z}=0. \quad (18)$$

The system [Eqs. (12)–(18)] is closed and self-consistently describes the dynamics of the SPP waves in graphene (single layer, bilayer, multilayer). S is the area of graphene layer, $F_{A_i}(z,\mathbf{q})=\int\exp(-i\mathbf{q}\mathbf{r}_\perp)|\phi_{A_i}(\mathbf{r})|^2\mathrm{d}\mathbf{r}_\perp$, and $F_{B_i}(z,\mathbf{q})=\int\exp(-i\mathbf{q}\mathbf{r}_\perp)|\phi_{B_i}(\mathbf{r})|^2\mathrm{d}\mathbf{r}_\perp$ are carbon atom form factors;

$$\mathbf{j}^{A_iB_i}_{\alpha}(z,\mathbf{q})=\int\exp(-i\mathbf{q}\mathbf{r})[\phi_{A_i}(\mathbf{r})\hat{\mathbf{p}}\phi_{B_i}(\mathbf{r}-\delta_\alpha)-\phi_{B_i}(\mathbf{r}-\delta_\alpha)\hat{\mathbf{p}}\phi_{A_i}(\mathbf{r})]\mathrm{d}\mathbf{r}_\perp, \quad (19)$$

are hopping currents between nearest graphene neighbor atoms, $\boldsymbol{\delta}_\alpha$ are distances to near neighbors in graphene,

$$B^{s_1 s_2}_{\mathbf{k}_1\mathbf{k}_2}(\mathbf{q},\omega)=\sum_j\left\{\frac{\int\mathrm{d}z\Phi(z,\mathbf{q},\omega)[c^{A_j*}_{\mathbf{k}_1 s_1}c^{A_j}_{\mathbf{k}_2 s_2}F_{A_j}(z,-\mathbf{q})+c^{B_j*}_{\mathbf{k}_1 s_1}c^{B_j}_{\mathbf{k}_2 s_2}F_{B_j}(z,-\mathbf{q})]}{\omega+E_{\mathbf{k}_2 s_2}-E_{\mathbf{k}_1 s_1}} -\frac{\sum_\alpha(c^{A_j*}_{\mathbf{k}_1 s_1}c^{B_j}_{\mathbf{k}_2 s_2}e^{i\mathbf{k}_2\delta_\alpha}-c^{B_j*}_{k_1 s_1}c^{A_j}_{k_2 s_2}e^{-i\mathbf{k}_1\delta_\alpha})\int\mathrm{d}z\mathbf{A}(z,\mathbf{q},\omega)\mathbf{j}^{A_jB_j}_{\alpha}(z,-\mathbf{q})}{2mc(\omega+E_{\mathbf{k}_2 s_2}-E_{\mathbf{k}_1 s_1})}\right\}. \quad (20)$$

3 Boundary Conditions and Dispersion Equations

The system [Eqs. (12)–(18)] has integro-differential form. They can be reduced to the system of homogeneous integral Fredholm equations. It was shown in Ref. 23 that for long-wave case when $qa\ll 1$ (a is graphene constant), the effective boundary conditions[17] give the same results. Using this approach, the potentials are continuous when crossing the graphene layers and derivative of potentials are discontinuous. The step of discontinuity is defined by integration of Eqs. (16) and (17) over thin region near the graphene layers $z_i-0<z<z_i+0$:

$$\Phi|_{z=z_i+0}=\Phi|_{z=z_i-0}, \quad (21)$$

$$\left.\frac{\mathrm{d}\Phi}{\mathrm{d}z}\right|_{z=z_i+0}-\left.\frac{\mathrm{d}\Phi}{\mathrm{d}z}\right|_{z=z_i-0}=-\sum\nolimits_{i'}(Z^{\Phi\Phi}_{ii'}\Phi+Z^{\Phi A_q}_{ii'}A_q)\Big|_{z=z_{i'}}, \quad (22)$$

$$A_q|_{z=z_i+0}=A_q|_{z=z_i-0}, \quad (23)$$

$$\left.\frac{\mathrm{d}A_q}{\mathrm{d}z}\right|_{z=z_i+0}-\left.\frac{\mathrm{d}A_q}{\mathrm{d}z}\right|_{z=z_i-0}=-\sum\nolimits_{i'}(Z^{A_q\Phi}_{ii'}\Phi+Z^{A_qA_q}_{ii'}A_q)\Big|_{z=z_{i'}}. \quad (24)$$

Here

$$Z_{ii'}^{\Phi\Phi} = \frac{4\pi e^2}{S}\sum_{1,2}\boldsymbol{\delta}_{\mathbf{k}_2+\mathbf{q},\mathbf{k}_1}(c_{\mathbf{k}_2 s_2}^{A_i *}c_{\mathbf{k}_1 s_1}^{A_i} + c_{\mathbf{k}_2 s_2}^{B_i *}c_{\mathbf{k}_1 s_1}^{B_i})\frac{c_{\mathbf{k}_1 s_1}^{A_{i'} *}c_{\mathbf{k}_2 s_2}^{A_{i'}} + c_{\mathbf{k}_1 s_1}^{B_{i'} *}c_{\mathbf{k}_2 s_2}^{B_{i'}}}{\omega + E_{\mathbf{k}_2 s_2} - E_{\mathbf{k}_1 s_1}} \times (n_{\mathbf{k}_2 s_2} - n_{\mathbf{k}_1 s_1}) \tag{25}$$

$$Z_{ii'}^{\Phi A_\mathbf{q}} = -\frac{4\pi e^2}{S}\sum_{1,2}\boldsymbol{\delta}_{\mathbf{k}_2+\mathbf{q},\mathbf{k}_1}(c_{\mathbf{k}_2 s_2}^{A_i *}c_{\mathbf{k}_1 s_1}^{A_i} + c_{\mathbf{k}_2 s_2}^{B_i *}c_{\mathbf{k}_1 s_1}^{B_i})(n_{\mathbf{k}_2 s_2} - n_{\mathbf{k}_1 s_1}) \times \frac{\sum_\alpha (c_{k_1}^{A_{i'} *}c_{k_2}^{B_{i'}} e^{i\mathbf{k}_2\delta_\alpha} - c_{k_1}^{B_{i'} *}c_{k_2}^{A} e^{-i\mathbf{k}_1\delta_\alpha})\int \mathrm{d}z\mathbf{q}\mathbf{j}_\alpha^{A_{i'}B_{i'}}(z,-\mathbf{q})}{2mcq(\omega + E_{k_2 s_2} - E_{k_1 s_1})} \tag{26}$$

$$Z_{ii'}^{A_\mathbf{q}A_\mathbf{q}} = \frac{2\pi e^2}{mcqS}\sum_{1,2,\alpha}\delta_{\mathbf{k}_2+\mathbf{q},\mathbf{k}_1}(n_{\mathbf{k}_2 s_2} - n_{\mathbf{k}_1 s_1})(c_{\mathbf{k}_2}^{A_i *}c_{\mathbf{k}_1}^{B_i} e^{i\mathbf{k}_1\delta_\alpha} - c_{\mathbf{k}_2}^{B_i *}c_{\mathbf{k}_1}^{A_i} e^{-i\mathbf{k}_2\delta_\alpha})\int \mathrm{d}z\mathbf{q}\mathbf{j}_\alpha^{A_iB_i}(z,\mathbf{q}) \times \frac{\sum_{\alpha'} (c_{k_1}^{A_{i'} *}c_{k_2}^{B_{i'}} e^{i\mathbf{k}_2\delta_{\alpha'}} - c_{k_1}^{B_{i'} *}c_{k_2}^{A} e^{-i\mathbf{k}_1\delta_{\alpha'}})\int \mathrm{d}z\mathbf{q}\mathbf{j}_{\alpha'}^{A_{i'}B_{i'}}(z,-\mathbf{q})}{2mcq(\omega + E_{k_2 s_2} - E_{k_1 s_1})} \tag{27}$$

$$Z_{ii'}^{A_\mathbf{q}\Phi} = -\frac{2\pi e^2}{mcqS}\sum_{1,2,\alpha}\delta_{\mathbf{k}_2+\mathbf{q},\mathbf{k}_1}(c_{\mathbf{k}_2}^{A_i *}c_{\mathbf{k}_1}^{B_i} e^{i\mathbf{k}_1\delta_\alpha} - c_{\mathbf{k}_2}^{B_i *}c_{\mathbf{k}_1}^{A_i} e^{-i\mathbf{k}_2\delta_\alpha}) \times (n_{\mathbf{k}_2 s_2} - n_{\mathbf{k}_1 s_1})\frac{c_{\mathbf{k}_1 s_1}^{A_{i'} *}c_{\mathbf{k}_2 s_2}^{A_{i'}} + c_{\mathbf{k}_1 s_1}^{B_{i'} *}c_{\mathbf{k}_2 s_2}^{B_{i'}}}{\omega + E_{\mathbf{k}_2 s_2} - E_{\mathbf{k}_1 s_1}}\int \mathrm{d}z\mathbf{q}\mathbf{j}_\alpha^{A_iB_i}(z,\mathbf{q}). \tag{28}$$

Using Eqs. (21)–(24), we obtain the following dispersion equation for single layer graphene:

$$(2\kappa - Z_{11}^{\Phi\Phi})(2\kappa - Z_{11}^{A_\mathbf{q}A_\mathbf{q}}) - Z_{11}^{\Phi A_\mathbf{q}}Z_{11}^{A_\mathbf{q}\Phi} = 0, \tag{29}$$

where $\kappa = \sqrt{q^2 - \omega^2/c^2}$. The π-electrons which contribute to the graphene dielectric function are nonrelativistic ($v_F \sim c/300$). Correspondingly, we further consider the electrons moving in graphene with nonrelativistic speeds. Besides, a part of the dielectric function corresponding to the vector potential is proportional to overlap integrals. Neglecting terms which contain these infinitesimals ($Z_{ii'}^{\Phi A_\mathbf{q}}, Z_{ii'}^{A_\mathbf{q}A_\mathbf{q}}, Z_{ii'}^{A_\mathbf{q}\Phi}$), the standard equation for SPP waves in single-layer graphene is obtained:

$$1 - \frac{Z_{11}^{\Phi\Phi}}{2\kappa} = 0. \tag{30}$$

Taking into account the correspondence $Z_{11}^{\Phi\Phi} = 4\pi e^2\Pi$, the above equation coincides with that derived in Ref. 24 [see Eqs. (1) and (3)]. Under the derivation of Eq. (30), the normalization of wave function and smallness of the SPP wave number $|q/k| \ll 1$ were used, which allowed the following approximations: $c_{\mathbf{k}_1 s_1}^{A*}c_{\mathbf{k}_2 s_1}^{A} + c_{\mathbf{k}_1 s_1}^{B*}c_{\mathbf{k}_2 s_1}^{B} \approx c_{\mathbf{k}_1 s_1}^{A*}c_{\mathbf{k}_1 s_1}^{A} + c_{\mathbf{k}_1 s_1}^{B*}c_{\mathbf{k}_1 s_1}^{B} = 1$. Note also that only intraband transitions have been taken into account.

In the case $k_F a \ll 1$, the doping electrons are in the vicinity of the Dirac point and the SPP wave dispersion Eq. (30) can be rewritten as

$$1 = \frac{4e^2}{\hbar v_F}k_F\frac{\omega - (\omega^2 - v_F^2 q^2)^{1/2}}{\kappa(\omega^2 - v_F^2 q^2)^{1/2}}. \tag{31}$$

Equation (31) is transformed into expressions derived in Ref. 24 if the SPP wave phase speed exceeds considerably the Dirac electron speed, i.e., the inequality $v_{\mathrm{ph}} \gg v_F$ holds true.

For a graphene bilayer (Fig. 1) the field can be written in the following form:

$$\Phi(z,\mathbf{q},\omega) = \begin{cases} a_1\exp(\kappa z), & z < 0 \\ b_1\exp(\kappa z) + b_2\exp(-\kappa z), & 0 < z < d \\ a_2\exp[-\kappa(z-d)], & z > d \end{cases}, \tag{32}$$

where d is the distance between graphene layers, $a_{1,2}$ and $b_{1,2}$ are coefficients to be determined from the boundary conditions [Eqs. (21)–(24)], which are rewritten as:

$$\begin{aligned} b_1 + b_2 &= a_1 \\ \kappa b_1 - \kappa b_2 - \kappa a_1 &= -Z_{11}^{\Phi\Phi} a_1 - Z_{12}^{\Phi\Phi} a_2 \\ b_1 e^{\kappa d} + b_2 e^{-\kappa d} &= a_2 \\ \kappa a_2 + \kappa b_1 e^{\kappa d} - \kappa b_2 e^{-\kappa d} &= Z_{22}^{\Phi\Phi} a_2 + Z_{21}^{\Phi\Phi} a_1. \end{aligned} \tag{33}$$

There is a possibility to provide an additional slowing of the electromagnetic wave in bilayer structures due to the low-frequency out-of-phase SPP wave mode (the acoustic SPP wave).[25] However, the slowing effect is suppressed by interlayer tunneling: In the presence of tunneling, the out-of-phase SPP wave mode develops a long-wavelength gap (a depolarization shift).[25] Bigraphene has four π bands. In undoped bigraphene two of these zones are fully occupied. If the Fermi level of doped bigraphene is below 0.4 eV, the doping electrons fill in the third π-band with the energy:

$$E = \sqrt{\gamma_0'^2 |f(k_x, k_y)|^2 + \frac{\gamma_1'^2}{2} - \gamma_1' \sqrt{\gamma_0'^2 |f(k_x, k_y)|^2 + \frac{\gamma_1'^2}{4}}}, \tag{34}$$

where γ_0' is the hopping between nearest neighbors in graphene plane, γ_1' is hopping between planes. In this case boundary conditions [Eq. (33)] for in-phase mode (optical SPP wave) of bilayer graphene gives the following SPP wave dispersion equation:

$$1 = \frac{\pi e^2}{\kappa S} \sum_{\mathbf{k}_1, \mathbf{k}_2} \delta_{\mathbf{k}_2 + \mathbf{q}, \mathbf{k}_1} \frac{n_{\mathbf{k}_2 s} - n_{\mathbf{k}_1 s}}{\omega + E_{\mathbf{k}_2 s} - E_{\mathbf{k}_1 s}} (1 + e^{-d\kappa}). \tag{35}$$

The SPP wave dispersion equation in this case gives optical mode similar to optical mode in single-layer graphene. Using the approximate energy dependence in the vicinity of the Dirac point for bigraphene as $\hbar^2 v_F^2 k^2 / \gamma_1'$ we reduce Eq. (35) to the form:

$$1 = \frac{2e^2}{\kappa \gamma_1'} (\hbar k_F)^2 \frac{q^2 v_F^2}{\omega^2}. \tag{36}$$

The spatially separated double-layer graphene in which tunneling is negligible can be used for achieving a large wave deceleration. In such systems the quantum wave function of electron state is concentrated near one of the layers. Therefore, the boundary conditions [Eq. (33)] can be written as:

$$\begin{aligned} b_1 + b_2 &= a_1 \\ \kappa b_1 - \kappa b_2 - \kappa a_1 &= -Z_{11}^{\Phi\Phi} a_1 \\ b_1 e^{\kappa d} + b_2 e^{-\kappa d} &= a_2 \\ \kappa a_2 + \kappa b_1 e^{\kappa d} - \kappa b_2 e^{-\kappa d} &= Z_{22}^{\Phi\Phi} a_2. \end{aligned} \tag{37}$$

Correspondingly, the dispersion equation is given by:

$$(2\kappa - Z_{11}^{\Phi\Phi})(2\kappa - Z_{22}^{\Phi\Phi}) - Z_{11}^{\Phi\Phi} Z_{22}^{\Phi\Phi} e^{-2\kappa d} = 0, \tag{38}$$

where

$$Z_{ii}^{\Phi\Phi} = \frac{4e^2}{\hbar v_F} k_{iF} \frac{\omega - (\omega^2 - v_F^2 q^2)^{1/2}}{(\omega^2 - v_F^2 q^2)^{1/2}}, \tag{39}$$

and k_{iF} are the Fermi momentums for layers $i = 1, 2$. The dispersion equation [Eq. (38)] with coefficients [Eq. (39)] is reduced to the dispersion equation obtained in Ref. 26 in the limit

$\omega \gg v_F q$. Because we are interested in a large wave deceleration, accounting for this difference is very important.

4 Discussion

The slowing of an electromagnetic wave described in previous sections is a crucial effect for the Čerenkov radiation mechanism. Figure 2 demonstrates the dependence $\omega(q)$ in the THz range, whereas Fig. 3 presents the ratio of the electromagnetic wave phase speed to the speed of light in a vacuum. One can see that the deceleration for single layer graphene is not too large and strongly depends on the density of doping electrons. It is seen that the slowing down in a single-layer graphene is 3 to 5 times at the typical electron doping $\sim 10^{12}$ cm^{-2}. Such values of the deceleration allow synchronization with an electron beam with the several tens of kilovolt energy. It is clear that the synchronization regime is nonreachable in single-layer graphene at reasonable densities. For the Čerenkov radiation by electrons with smaller energies, and particulary with nonrelativistic electron energies, corresponding to the electron bands in graphene, a

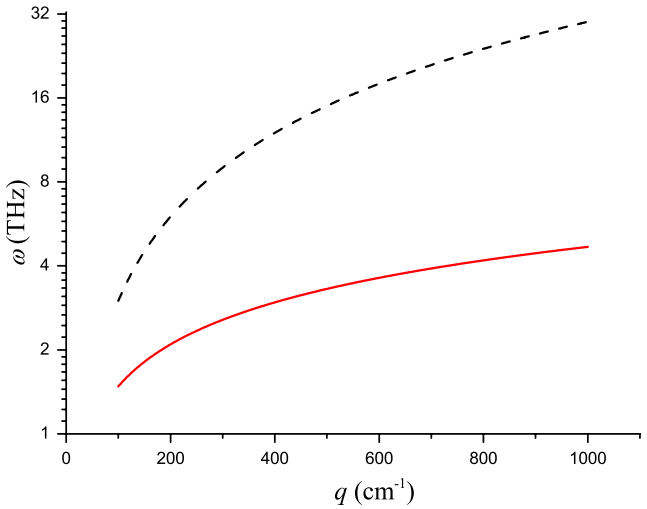

Fig. 2 The electromagnetic wave frequency ω (l/s) versus wave number q (l/cm) for single layer graphene (the red curve). The dash curve shows the light line. Logarithmic scale of vertical axis was used.

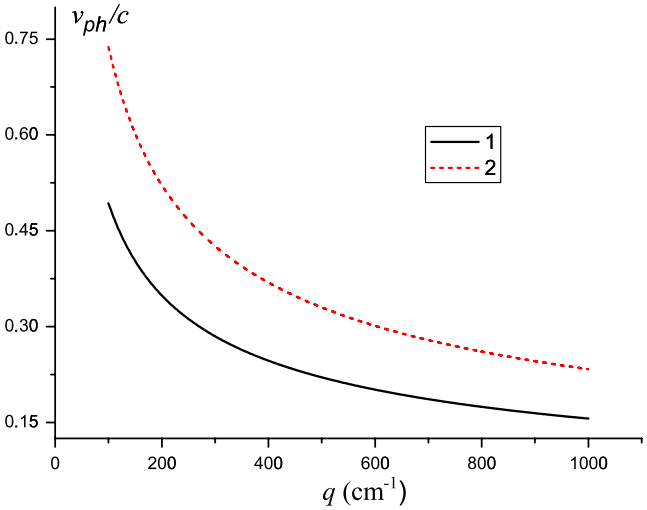

Fig. 3 The SPP wave phase speed v_{ph}/c versus the wave number q (1/cm) in a single-layer graphene for the densities (1) 10^{12} cm^{-2} and (2) 5×10^{12} cm^{-2} of the doping electrons.

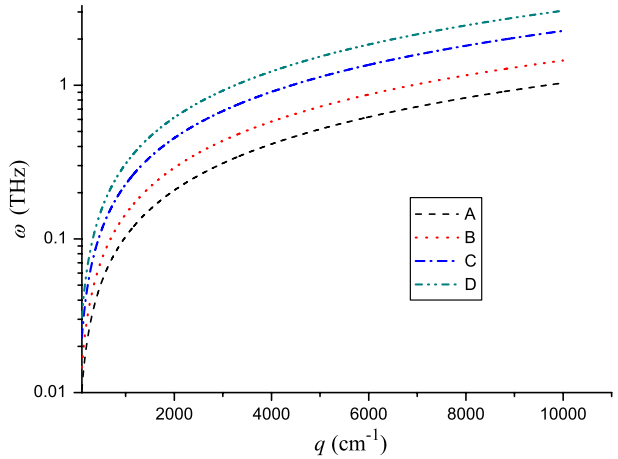

Fig. 4 The frequency ω versus the wave number q for two spatially expanded graphene monolayers: the distance d between layers is (A) 4 nm, (B) 30 nm, (C) 100 nm, and (D) 200 nm for doping electron densities $n_1 = n_2 = 10^{12}$ cm^{-2}.

stronger deceleration is required (up to 300 times). Such slowing can be reached in bilayer and multilayer graphene structures for acoustic-type modes. The tunneling between graphene layers can suppress the strong slowing effect in multilayer structures, therefore reducing the tunneling is extremely desirable.

A spatially separated double-layer graphene monolayer with suppressed inter-layer tunneling is a suitable candidate for this purpose. Figure 4 shows the frequency dependence on the wave number for different inter-layer distances. The plots are obtained using Eqs. (38) and (39). The slowing down up to the speed of π-electron can be reached in such structures. The spatially expanded double-layer graphene has also another useful property: the frequency and the phase speed appear to be tunable due to independent control of carrier densities n_1 and n_2 in the monolayers and the interlayer separation d.

5 Conclusion

The self-consistent equations describing SPP wave dynamics in multilayer graphene have been derived and analyzed. The SPP wave dispersion law obtained from these equations has been investigated to provide synchronization between the electromagnetic wave and the electron beam, i.e., to achieve proximity of the electromagnetic wave phase speed to the Dirac electron speed in graphene v_F. It has been shown that the multi (double-) layer graphene nanoplatelets, especially in the spatially separated double-layer graphene, allows such a proximity and thus are promising candidates for the nano-sized Čerenkov-type THz emitters. The development of such emitters is a challenging problem of present-day nanoelectronics and nanophotonics.

Acknowledgments

This research was partially supported by EU FP7 under Projects FP7-230778 TERACAN, FP7-247007 CACOMEL and FP7-PEOPLE-2012-IRSES FAEMCAR. The problem statement as well as writing of the paper was done jointly by K. Batrakov and S. Maksimenko. Analytical and numerical calculations were carried out by K. Batrakov and V. Saroka. Analysis and discussion of results were performed jointly by K. Batrakov, Ch. Thomsen and S. Maksimenko. All authors made equal intellectual contribution to this paper.

References

1. S. Iijima, "Helical microtubules of graphitic carbon," *Nature* **354**, 56–58 (1991), http://dx.doi.org/10.1038/354056a0.

2. R. Saito, G. Dresselhaus, and M. S. Dresselhaus, *Physical Properties of Carbon Nanotubes*, Imperial College Press, London (1998).
3. S. Reich, C. Thomsen, and J. Maultzsch, *Carbon Nanotubes: Basic Concepts and Physical Properties*, Wiley, Berlin (2004).
4. D. Dragoman and M. Dragoman, "Terahertz fields and applications," *Prog. Quantum Electron.* **28**(1), 1–66 (2004), http://dx.doi.org/10.1016/S0079-6727(03)00058-2.
5. D. Dragoman and M. Dragoman, "Terahertz oscillations in semiconducting carbon nanotube resonant-tunnelling diodes," *Physica E* **24**(3–4), 282–289 (2004), http://dx.doi.org/10.1016/j.physe.2004.05.001.
6. D. Dragoman and M. Dragoman, "Terahertz continuous wave amplification in semiconductor carbon nanotubes," *Physica E* **25**(4), 492–496 (2005), http://dx.doi.org/10.1016/j.phsyse.2004.08.001.
7. O. V. Kibis and M. E. Portnoi, "Carbon nanotubes: a new type of emitter in the terahertz range," *Tech. Phys. Lett.* **31**(8), 671–673 (2005), http://dx.doi.org/10.1134/1.2035361.
8. O. V. Kibis, M. Rosenau da Costa, and M. E. Portnoi, "Generation of terahertz radiation by hot electrons in carbon nanotubes," *Nano Lett.* **7**(11), 3414–3417 (2007), http://dx.doi.org/10.1021/nl0718418.
9. G. Y. Slepyan et al., "Theory of optical scattering by achiral carbon nanotubes, and their potential as optical nanoantennas," *Phys. Rev. B* **73**(19), 195416 (2006), http://dx.doi.org/10.1103/PhysRevB.73.195416.
10. F. Rana, "Graphene terahertz plasmon oscillators," *IEEE Trans. Nanotech.* **7**(1), 91–99 (2008), http://dx.doi.org/10.1109/TNANO.2007.910334.
11. K. G. Batrakov, P. P. Kuzhir, and S. A. Maksimenko, "Radiative instability of electron beam in carbon nanotubes," *Proc. SPIE* **6328**, 632801 (2006), http://dx.doi.org/10.1117/12.678029.
12. K. G. Batrakov et al., "Carbon nanotube as a Cherenkov-type light emitter and free electron laser," *Phys. Rev. B* **79**(12), 125408 (2009), http://dx.doi.org/10.1103/PhysRevB.79.125408.
13. K. G. Batrakov, P. P. Kuzhir, and S. A. Maksimenko, "Toward the nano-FEL: undulator and Cherenkov mechanisms of light emission in carbon nanotubes," *Physica E* **40**(5), 1065–1068 (2008), http://dx.doi.org/10.1016/j.physe.2007.08.003.
14. K. G. Batrakov, P. P. Kuzhir, and S. A. Maksimenko, "Stimulated emission of electron beam in nanotube bundles," *Physica E* **40**(7), 2370–2374 (2008), http://dx.doi.org/10.1016/j.physe.2007.07.029.
15. K. G. Batrakov et al., "Terahertz processes in carbon nanotubes," *J. Nanophoton.* **4**(1), 041665 (2010), http://dx.doi.org/10.1117/1.3436585.
16. K. G. Batrakov, P. P. Kuzhir, and S. A. Maksimenko, "Cherenkov synchronism: non-relativistic electron beam in multi-walled nanotube and multi-layer graphene," *Physica B: Condensed Matter* **405**(14), 3050–3053 (2010), http://dx.doi.org/10.1016/j.physb.2010.01.047.
17. G. Y. Slepyan et al., "Electrodynamics of carbon nanotubes: dynamic conductivity, impedance boundary conditions, and surface wave propagation," *Phys. Rev. B* **60**(24), 17136–17149 (1999), http://dx.doi.org/10.1103/PhysRevB.60.17136.
18. S. A. Mikhailov and K. Ziegler, "New electromagnetic mode in graphene," *Phys. Rev. Lett.* **99**(1), 016803 (2007), http://dx.doi.org/10.1103/PhysRevLett.99.016803.
19. A. Hill, S. A. Mikhailov, and K. Ziegler, "Dielectric function and plasmons in graphene," *Europhys. Lett.* **87**(2), 27005 (2009), http://dx.doi.org/10.1209/0295-5075/87/27005.
20. M. Jablan, H. Buljan, and M. Soljacic, "Transverse electric plasmons in bilayer graphene," *Opt. Express* **19**(12), 11236–11241 (2011), http://dx.doi.org/10.1364/OE.19.011236.
21. V. B. Berestetskii, E. M. Lifshitz, and L. P. Pitaevskii, *Quantum Electrodynamics*, Oxford, Butterworth-Heinemann (1997).
22. B. Partoens and F. M. Peeters, "From graphene to graphite: electronic structure around the K point," *Phys. Rev. B* **74**(7), 075404 (2006), http://dx.doi.org/10.1103/PhysRevB.74.075404.
23. K. G. Batrakov, P. P. Kuzhir, and S. A. Maksimenko, "Electromagnetic wave slowing down in graphene bilayer," in *AIP Conf. Proc.*, Vol. **1176**, pp. 40–42 (2009).
24. S. Das Sarma and E. H. Hwang, "Collective modes of the massless Dirac plasma," *Phys. Rev. Lett.* **102**(20), 206412 (2009), http://dx.doi.org/10.1103/PhysRevLett.102.206412.

25. S. Das Sarma and E. H. Hwang, "Plasmons in coupled bilayer structures," *Phys. Rev. Lett.* **81**(19), 4216–4219 (1998), http://dx.doi.org/10.1103/PhysRevLett.81.4216.
26. E. H. Hwang and S. Das Sarma, "Plasmon modes of spatially separated double-layer graphene," *Phys. Rev. B* **80**(20), 205405 (2009), http://dx.doi.org/10.1103/PhysRevB.80.205405.

Konstantin G. Batrakov is a senior researcher at the Institute for Nuclear Problems and an associate professor at Belarus State University, Minsk, Belarus. He received his PhD in Theoretical Physics in 1993 from the Institute for Nuclear Problems, Minsk, Belarus. He has carried out research for more than 20 years. The results, obtained by Dr. Batrakov in coauthorship with his colleagues in the field of Free Electron Lasers have been used in the first lasing of Volume free electron laser in the Institute for Nuclear Problems. His present research interest is possible nanotubes applications as monomolecular light emitters in the THz frequency region (nano-scale free electron laser).

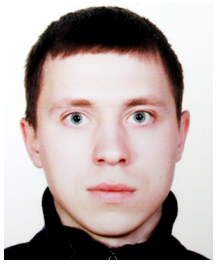

Vasily A. Saroka received his Masters degree from the Physics Department of Belorussian State University in 2012. He works at the Institute for Nuclear Problems. His field of scientific interests includes graphene-like structures, plasmon, and plasmon-polariton excitations of such structures. He has several publications concerning these fields.

Sergey A. Maksimenko received an MS degree in physics of heat and mass transfer in 1976, and a PhD degree in theoretical physics in 1988, both from Belarusian State University (BSU), Minsk, Belarus, and a Doctor of Science degree in theoretical physics in 1996 from the Institute of Physics, Belarus National Academy of Science. Since 1992 he has been working as head of the Laboratory of Electrodynamics of Nonhomogeneous Media at the Research Institute for Nuclear Problems, BSU. He also teaches at the BSU physical department. He has authored or coauthored more than 150 conference and journal papers. He is a chair of the international conference Fundamental and Applied Nanoelectromagnetics conference in Minsk, May 2012. He is SPIE Fellow and is the Associate Editor of the Journal of Nanophotonics. His current research interests are electromagnetic wave theory and electromagnetic processes in quasione- and zero-dimensional nanostructures in condensed matter and nanocomposites with the focus on nanocarbon. He participates in a number of international research projects, coordinator of EU FP7 project FP7-226529 BY-NANOERA.

Christian Thomsen has been full professor since 1994 at the Technische Universitat, Berlin, where he is currently chairman of the mathematics and natural science faculty. His research focus is on the optical properties of carbon nanotubes. He has authored about 400 publications and has been organizing the International Winterschool on the Electronic Properties of Novel Materials (IWEPNM) since 2007.